Significance of *J* and CTOD estimation procedures for common fracture specimens: the SE(T) configuration revisited

Claudio Ruggieri

Fracture Mechanics and Structural Integrity Laboratory
Department of Naval Architecture and Ocean Engineering, University of São Paulo, São Paulo (Brazil)
claudio.ruggieri@usp.br

ABSTRACT. This study addresses further developments of the evaluation procedure for J and CTOD in common fracture specimens based upon the η-method. Very detailed non-linear finite element analyses for plane-strain models provide the evolution of load with increased load-displacement to define the relationship between plastic work and crack-tip driving force (J and CTOD) from which the η-values are derived. Further analyses based on the load separation method are also conducted to define alternative η-values against which factors η evaluated from plastic work can be compared. The analyses reveal that η-factors based on load-line displacement (LLD) are sensitive to plasticity changes at locations remote from the crack-tip region. Overall, the present results provide a strong support to use η-based procedures in toughness measurements for conventional SE(T) fracture specimens.

KEYWORDS. J-integral; CTOD; eta-factor; SE(T) specimen; Load separation.

INTRODUCTION

Standardized techniques for crack growth resistance testing of structural steels, including ASTM E1820 [1] standard, routinely employ three-point bend SE(B) and compact tension C(T) specimens containing deep, through cracks ($a/W \geq 0.45{\sim}0.5$). The primary motivation to use deeply cracked specimens is to guarantee conditions leading to crack growth under high crack-tip constraint with limited-scale plasticity. For these specimens, the advancing near-tip region over which elastic unloading and strongly nonproportional loading takes place is well contained within the J-dominance zone ahead of the crack tip [2]. However, a variety of crack-like defects are most often surface cracks formed during in-service operation and exposure to aggressive environment or during welding fabrication. Structural components falling into this category include girth welds made in field conditions for high pressure piping systems and steel catenary risers. These crack configurations generally develop low levels of crack-tip stress triaxiality which contrast sharply to conditions present in deeply cracked specimens [3]. Recent defect assessment procedures now under development advocate the use of geometry dependent fracture toughness values so that crack-tip constraint in the test specimen closely matches crack-tip constraint in the structural component. In particular, fracture toughness values measured using single edge notch tension (SE(T)) specimens appear more applicable for characterizing the fracture resistance of pressurized pipelines and cylindrical vessels than standard, deep notch fracture specimens under bend loading [4, 5].

Current evaluation procedures for J focus primarily on developing estimation schemes for its plastic component, denoted J_p. These methodologies have evolved essentially along two lines of development: (1) estimation procedures relating the plastic contribution to the strain energy and J; (2) fully plastic descriptions of J based upon HRR-

controlled crack-tip fields and limit load solutions. The first approach employs a plastic η-factor introduced by Sumpter and Turner [6] to relate the macroscale crack driving forces (J and CTOD) to the area under the load versus load line displacement (or crack mouth opening displacement) for cracked configurations. Because of its relative ease with which the load-displacement records can be measured in conventional test specimens, the method is most suited for testing protocols measuring fracture toughness such as ASTM E1820 [1]. The second approach derives from previous work of Kumar et al. [7] to introduce an estimation procedure for J_p applicable to elastic-plastic materials following a power hardening law such as the Ramberg-Osgood (R-O) model [8]. Here, J_p is expressed in the general form $J_p \propto h_1\left(a/W, \ell, n\right) \times \left(\Lambda/\Lambda_0\right)^{n+1}$ where a is the crack size, W denotes the component width, ℓ represents a characteristic length for the cracked component, n is the R-O strain hardening exponent, Λ defines a generalized load and Λ_0 is the corresponding (plastic) limit load. Factor h_1 represents a nondimensional parameter dependent upon crack size, component geometry and strain hardening properties which simply scales J_p with $\left(\Lambda/\Lambda_0\right)^{n+1}$. The method became widely known as the EPRI methodology and has later been expanded by Zahoor [9] to include additional geometries such as circumferentially and axially cracked pipes under tensile and bending loads. Another related approach to determine J from load-displacement records which shares much in common with the previous outlined methodology based on η-factors adopts a load separation analysis proposed by Paris et al. [10] to evaluate for conventional fracture specimens. Here, a key assumption is that load can be represented as the product of a crack geometry function (G) and a material deformation function (D) so that factor $\eta \propto G\left(a/W\right)$. Sharobeam and Landes [11] employed the load separation concept to develop an experimental procedure to determine η-factors for selected crack geometries.

While η-based procedures have proven very effective in estimation schemes for J and CTOD based on experimentally measured load-displacement records using deeply cracked specimens, there still exist some differences in η-values for low constraint fracture specimens. In particular, Sharobeam and Landes [11] have arrived at a set of solutions for η-values which is independent of the a/W-ratio. Because of the increased utilization of geometry dependent specimens in fracture toughness measurements and defect assessment procedures applicable to low constraint crack configurations, these differences may concern potential users and experimentalists who rely on η-based methods to measure J and CTOD for these fracture specimens. Since a number of design and construction codes, including welding and material specifications, define minimum values of fracture toughness that need to be achieved to comply with their acceptance criteria, differences in the measured fracture toughness values can result in large economic consequences as well as unconservative structural integrity assessments.

Motivated by these observations, this study addresses further developments of the evaluation procedure for J and CTOD in common fracture specimens based upon the η-method. Very detailed non-linear finite element analyses for plane-strain models provide the evolution of load with increased load-displacement to define the relationship between plastic work and crack-tip driving force (J and CTOD) from which the η-values are derived. Further analyses based on the load separation method are also conducted to define alternative η-values against which factors evaluated from plastic work can be compared. The analyses reveal that η-factors based on load-line displacement (LLD) are sensitive to plasticity changes at locations remote from the crack-tip region. Overall, the present results provide a strong support to use η-based procedures in toughness measurements for conventional SE(T) fracture specimens.

ESTIMATION PROCEDURES FOR THE J INTEGRAL AND CTOD

This section provides the essential features of the analytical framework needed to determine J and CTOD for common fracture specimens based upon experimental measurements of load-displacement records with particular emphasis on the SE(T) configuration. The presentation begins with the J-integral and CTOD analysis for a cracked body based upon the plastic work measured from load-displacement records, LLD (Δ) and CMOD (V). Subsequent development focuses on a related procedure to evaluate J based upon the load separation analysis for cracked bodies. The description that follows also includes a J-integral evaluation scheme using multispecimen measurements of plastic work which enables direct comparisons with numerical J-values derived from domain integral procedures.

Experimental J and CTOD measurements based on plastic work

The energy release rate definition of J for a cracked body with thickness B illustrated in Fig. 1 provides the basis to estimate the J-integral for a stationary crack based upon measured load-load line displacement records. Consistent with deformation theory, the path-independent J-integral is given by [12-14]

$$J = \frac{1}{B}\int_0^P \left(\frac{\partial \Delta}{\partial a}\right)_P dP = -\frac{1}{B}\int_0^\Delta \left(\frac{\partial P}{\partial a}\right)_\Delta d\Delta \tag{1}$$

where P is the applied load, Δ is the load-line displacement (LLD) and a is the crack size. Here, it is understood that the above integrals correspond to load control and displacement control conditions.

(a)   (b)
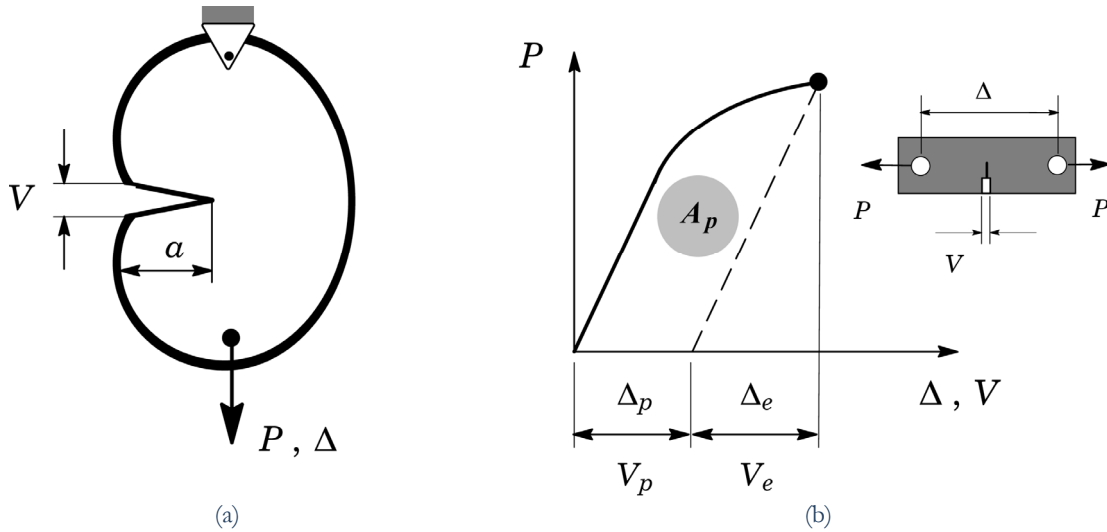
Figure 1: (a) Arbitrary cracked body with thickness B subjected to remote loading; (b) Definition of the plastic area under the load-displacement curve.

Upon consideration of the elastic, Δ_e, and plastic, Δ_p, components of the load line displacement given by

$$\Delta = \Delta_e + \Delta_p \tag{2}$$

and manipulating the first integral term of Eq. (1), J can be expressed as

$$J = \frac{1}{B}\int_0^P \left(\frac{\partial \Delta_e}{\partial a}\right)_P dP + \frac{1}{B}\int_0^P \left(\frac{\partial \Delta_p}{\partial a}\right)_P dP = J_e + J_p \tag{3}$$

where J_e and J_p are the elastic and plastic components. Here, J_e is conveniently defined by the energy release rate for a linear elastic cracked body under Mode I deformation in the standard form

$$J_e = \frac{K_I^2}{E'} \tag{4}$$

where K_I denotes the (Mode I) elastic stress intensity factor for the cracked configuration and $E' = E/(1-\nu^2)$ with E and ν denoting the (longitudinal) elastic modulus and Poisson's ratio.

The plastic component, J_p, is derived from adopting the approach proposed by Sumpter and Turner [6] building upon earlier work of Rice et al. [15] to relate the J-integral to the area under the load versus load-line displacement. Fig. 1(b) illustrates the essential features of the estimation procedure for J_p based upon LLD records measured using SE(T)

fracture specimens; the method is equally valid for other crack configurations. The approach simply relates the plastic contribution to the strain energy (due to the crack) and J in the form [12]

$$J_p = \frac{1}{B}\int_0^P \left(\frac{\partial \Delta_p}{\partial a}\right)_P dP = \frac{\eta_J^{LLD}}{Bb}\int_0^P P\, d\Delta_p = \frac{\eta_J^{LLD}\, A_p^{LLD}}{Bb} \tag{5}$$

where A_p^{LLD} is the plastic area under the load versus load line displacement, b is the uncracked ligament ($b = W - a$ where W is the specimen width and a is the crack length). To arrive at Eq. (5), the equality $da = -db$ was used. Factor η_J^{LLD} introduced by Sumpter and Turner [6] represents a nondimensional parameter which relates the plastic contribution to the strain energy for the cracked body with J and is assumed to be a function of the flawed configuration and independent of loading [12].

The specimen response (and, consequently , the plastic area under the load versus displacement curve) illustrated in Fig. 1(b) can also be defined in terms of crack mouth opening displacement (CMOD or V) data. For definiteness, the corresponding η_J-factor is denoted η_J^{CMOD} which enables expressing J_p as

$$J_p = \frac{\eta_J^{CMOD}\, A_p^{CMOD}}{Bb} \tag{6}$$

The previous framework also applies when the CTOD is adopted to characterize the crack-tip driving force. Following the earlier analysis for the J-integral and using the connection between J and the crack-tip opening displacement (δ) [16,17] given by

$$\delta = \frac{J}{m\sigma_{ys}} \tag{7}$$

in which m is a dimensionless constant, a formally similar expression to Eq. (3) is employed to yield

$$\delta = \delta_e + \delta_p \tag{8}$$

where the elastic component, δ_e, is now given by

$$\delta_e = \frac{K_I^2}{m_{ssy}\,\sigma_{ys}\,E'} \tag{9}$$

and the plastic component, δ_p, is expressed as

$$\delta_p = \frac{\eta_\delta^{CMOD}\, A_p^{CMOD}}{Bb\,\sigma_{ys}} \tag{10}$$

where factor η_δ^{CMOD} represents a nondimensional parameter which describes the effect of plastic strain energy on the applied CTOD. In the above expressions, σ_{ys} is the material's yield stress, m_{ssy} is a plastic constraint factor under small scale yielding (SSY) conditions [18] and parameter m represents a proportionality coefficient often used to relate to total value of J to the total value of CTOD and strongly dependent on material's strain hardening [16, 17]. When the CTOD is evaluated based on the plastic hinge model such as in BS 7448 standard [19], factor m_{ssy} is often assigned a value of 2.

Load Separation Analysis
An alternative approach to evaluate the plastic component of the J-integral, , from laboratory testing of conventional fracture specimens derives from the load separation method proposed by Paris et al. [10]. Based upon dimensional

analysis arguments, they proposed a separable form for the load, P, represented as the product of a crack geometry function (G) and a material deformation function (D) expressed by

$$P = G\left(\frac{a}{W}\right) \times D\left(\frac{\Delta_p}{W}\right) \tag{11}$$

To arrive at a convenient procedure to evaluate factor η_J based on the load separation concept, the above Eq. (11) is used in conjunction with the second integral of Eq. (1) so that the integral form of J_p resolves after some manipulation to

$$-\frac{1}{B}\int_0^{\Delta_p}\left\{\frac{\partial[G(a/W)D(\Delta_p/W)]}{\partial a}\right\}d\Delta_p = \frac{\eta_J^{LLD}}{Bb}\int_0^{\Delta_p}[G(a/W)D(\Delta_p/W)]d\Delta_p \tag{12}$$

By noting that the material deformation function, D, does not depend on crack size, Eq. (12) can be rearranged to define the plastic factor η_J^{LLD} in the form

$$\eta_J^{LLD} = -\frac{(b/W)}{G(a/W)} \times \frac{\partial G(a/W)}{\partial(a/W)} = \frac{(b/W)}{G(b/W)} \times \frac{\partial G(b/W)}{\partial(b/W)} \tag{13}$$

where it is understood that $\partial b = -\partial a$ and η_J depends only on the crack geometry function G.

The above resulting form of the load separation model to evaluate factor expressed by the above Eqs. (13) requires the knowledge (or, at least, a convenient choice) of the function G for the cracked configuration under analysis. Sharobeam and Landes [11] developed an experimental procedure to determine factor η_J for planar fracture specimens in which the crack geometry function G is described in terms of load-plastic displacement records for two specimens made of the same material and identical geometry and overall size but different crack length. Their analyses motivated the introduction of a separation parameter, S_k, defined as a ratio of load for specimens with different crack ligament measured at a fixed value of plastic displacement, Δ_p, in the form

$$S_k(b/W) = \left[\frac{P(b_k/W)}{P(b_0/W)}\right]_{\Delta_p} \tag{14}$$

where $P(b_k/W)$ and $P(b_0/W)$ are the load for specimens with crack ligament size b_k and b_0 in which subscript "0" represents a reference specimen size. For definiteness, this quantity is denoted S_k^{LLD}.

Following Sharobeam and Landes [11], introduction of parameter S_k allows a straightforward manner to determine the crack geometry function $G(b/W)$. Invoking the separable form of the load, P, given by previous Eq. (11), and noting again that the material deformation function, D, does not depend on crack size for a given plastic displacement, Δ_p, the above Eq. (14) can be rewritten as

$$S_k(b/W) = \left[\frac{G(b_k/W)}{G(b_0/W)}\right]_{\Delta_p} = \beta^{-1}[G(b_k/W)]_{\Delta_p} \tag{15}$$

where $\beta = [G(b_0/W)]_{\Delta_p}$ remains constant once a reference specimen size is adopted.

Consequently, the plastic η factors corresponding to LLD records can be expressed in terms of parameter S_k in the form

$$\eta_J^{LLD} = \frac{(b/W)}{S_k^{LLD}(b/W)} \times \frac{\partial S_k^{LLD}(b/W)}{\partial(b/W)} \tag{16}$$

in which now evaluation of factor η_J^{LLD} requires the knowledge (or, at least, a convenient choice) of the function for the cracked configuration under analysis. In subsequent section, a load separation analysis is explored for plane-strain models of pin-loaded and clamped SE(T) models to arrive at a set of η-values with increased a/W-ratios for these specimens based on different fitting functions for S_k.

J evaluation procedure using multispecimen measurements

A fundamental approach related to both of those previously described procedures to evaluate the J-integral derives directly from considering the variation in potential energy for a cracked body due to virtual crack extension. This concept forms the basis of the original work conducted by Begley and Landes [20] in which J was introduced as a fracture criterion.

Development of the evaluation procedure for J begins by considering its energy interpretation in the form

$$J = -\frac{1}{B}\frac{dU_p}{da} \tag{17}$$

where U_p is the potential energy for the cracked body and a is the crack size. By considering fracture specimens with identical geometry and configuration (W and B) but with different initial crack lengths, the area under the load-displacement curve for each specified displacement Δ_i illustrated in Fig. 2(a) enables the construction of the relationship between the potential energy and crack size as schematically represented in Fig. 2(b). Using the energy release rate definition expressed by previous Eq. (17), the J-integral with increased values of Δ for a given crack size, a, is simply evaluated from the derivative of U_p with respect to the crack size as evident from Fig. 2(b).

Begley and Landes [20] adopted the previously outlined procedure to determine J from experimentally measured load-displacement records using an extensive series of test specimens for an A533 pressure vessel steel at room temperature. The method requires testing a large number of specimens which makes routine laboratory evaluation of J a rather cumbersome task. Nevertheless, this approach will be pursued here in a numerical framework rather than an experimental procedure to evaluate J from load-displacement records against which the line integral definition of J can be compared.
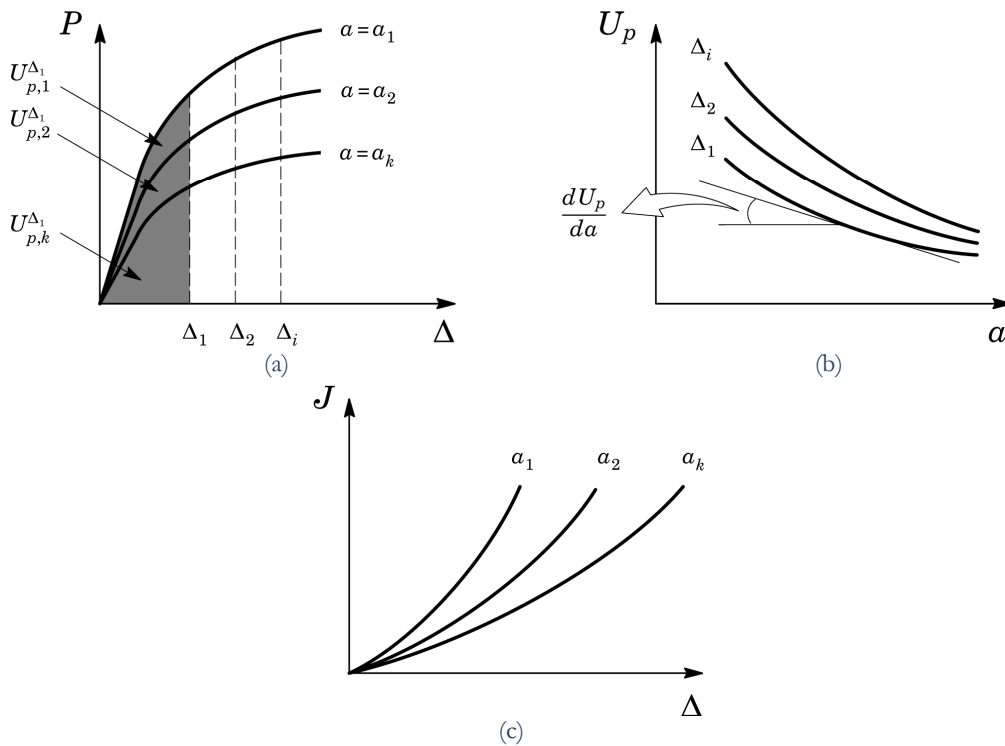
Figure 2: Scheme of the multispecimen procedure to evaluate the -integral proposed by Begley and Landes [20].

COMPUTATIONAL PROCEDURES AND FINITE ELEMENT MODELS

Plane-strain models of SE(T) fracture specimens

Nonlinear finite element analyses are described for plane-strain models of a wide range of conventional 1-T SE(T) fracture specimens (thickness $B = 25.4$ mm) under pin-loaded and clamped end conditions with $W/B = 2$. The analysis matrix includes SE(T) specimens having $a/W = 0.1$ to 0.7 with increments of 0.05, $H/W = 6$ (pin-loaded end) and $H/W = 10$ (clamped ends). Here, a is the crack size specimen, W is the specimen width and H is the distance between the pin loading or clamps. Fig. 3 shows the geometry and specimen dimensions for the analyzed crack configurations with different loading conditions, pin-loaded ends vs. clamped ends; these specimens are denoted as SE(T)$_P$ and SE(T)$_C$.

Fig. 4 shows the finite element models constructed for the plane-strain analyses of the pin-loaded SE(T) specimen having $a/W = 0.5$. All other crack models have very similar features. A conventional mesh configuration having a focused ring of elements surrounding the crack front is used with a small key-hole at the crack tip; the radius of the key-hole, ρ_0, is 0.0025 mm to enhance computation of J-values at low deformation levels. Previous numerical analyses [4-5] reveal that such mesh design provides detailed resolution of the near-tip stress-strain fields which is needed for accurate numerical evaluation of J-values. Symmetry conditions permit modeling of only one-half of the specimen with appropriate constraints imposed on the remaining ligament. A typical half-symmetric model has one thickness layer of ~1400 8-node, 3D elements (~3000 nodes) with plane-strain constraints ($w = 0$) imposed on each node.

These finite element models are loaded by displacement increments imposed on the loading points to enhance numerical convergence and to provide a closer correspondence with the actual experimental conditions at the specimen ends. Further, the numerical analyses for the pin-loaded specimen incorporate the contact interaction between the loading pin (represented as a rigid cylinder) and the specimen (see Fig. 4).
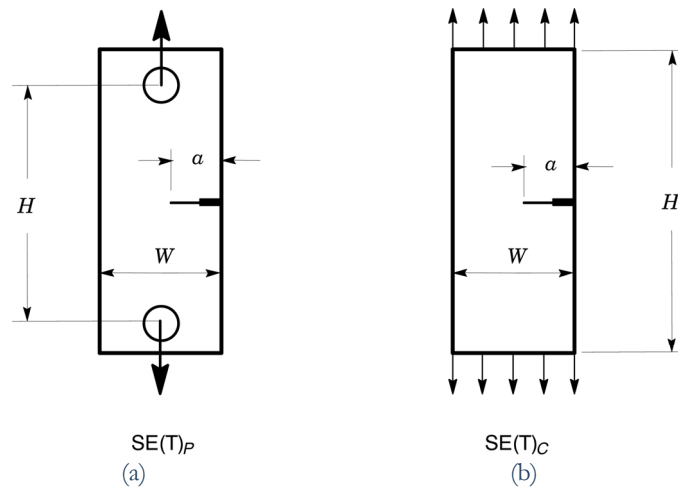
Figure 3: Geometries for analyzed SET fracture specimens: (a) Pin-loaded specimen; (b) Clamped specimen.
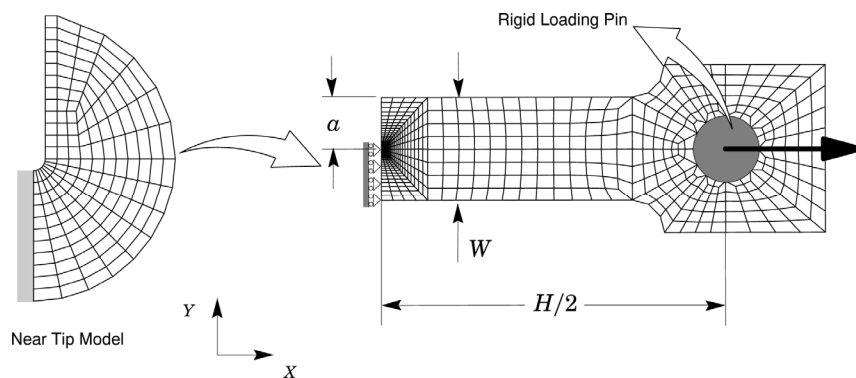
Figure 4: Finite element models used in plane-strain analysis of the pin-loaded SE(T) specimen with $a/W = 0.5$ and $H/W = 6$.

Material Models

Evaluation of factor η requires nonlinear finite element solutions which include the effects of plastic work on J and the load-displacement response. These analyses utilize an elastic-plastic constitutive model with J_2 flow theory and conventional Mises plasticity in small geometry change (SGC) setting. The numerical solutions employ a simple power-hardening model to characterize the uniaxial true stress ($\overline{\sigma}$) vs. logarithmic strain ($\overline{\varepsilon}$) in the form

$$\frac{\overline{\varepsilon}}{\varepsilon_{ys}} = \frac{\overline{\sigma}}{\sigma_{ys}} \qquad \overline{\varepsilon} \leq \varepsilon_{ys} \qquad ; \qquad \frac{\overline{\varepsilon}}{\varepsilon_{ys}} = \left(\frac{\overline{\sigma}}{\sigma_{ys}}\right)^n \qquad \overline{\varepsilon} > \varepsilon_{ys} \qquad (18)$$

where σ_{ys} and ε_{ys} are the reference (yield) stress and strain, and n is the strain hardening exponent. The finite element analyses consider material flow properties covering typical structural, pressure vessel and pipeline grade steels with $E = 206$ GPa and $\nu = 0.3$: $n = 5$ and $E/\sigma_{ys} = 800$ (high hardening material), $n = 10$ and $E/\sigma_{ys} = 500$ (moderate hardening material), $n = 20$ and $E/\sigma_{ys} = 300$ (low hardening material). These ranges of properties also reflect the upward trend in yield stress with the increase in strain hardening exponent, n, characteristic of ferritic structural steels, including pipeline steels.

Computational procedures

The finite element code WARP3D [21] provides the numerical solutions for the plane-strain analyses reported here. The code enables conventional linear elastic analysis and incorporates both a Mises (J_2) constitutive model in both small-strain and finite-strain framework. Evaluation of the J-integral derives from a domain integral procedure [22] which yields J-values retaining strong path independence for domains defined outside the highly strained material near the crack tip. Evaluation of the numerical value of CTOD follows the 90° procedure [18] to the deformed crack flanks. To avoid potential problems with the CTOD computation related to the severe mesh deformation at the crack tip, the approach adopted here defines the value of half the crack tip opening displacement as the intercept between a straight line at 45° from the crack tip (which is obtained by a linear regression of the corresponding nodal displacements) and a straight line passing through selected nodes at the crack flank.

The numerical simulation of the pin loading process involves the contact interaction between the loading pin (represented as a rigid cylinder) and the specimen. WARP3D uses a simple penalty method to enforce displacement constraints in the solution of the finite element model which creates springs at the contact points. The spring stiffness corresponds to the penalty parameter, while the amount of remaining penetration corresponds to the error in the enforcement of the constraint. WARP3D adds each spring stiffness into the corresponding element stiffness matrices instead of directly into the global stiffness matrix. The research code FRACTUS2D [23] is employed in all computations to determine factors η_J and η_δ as well as the load separation analyses and application of the multispecimen procedure for the cracked configurations described here.

RELATIONSHIP BETWEEN J AND PLASTIC WORK

B efore undertaking evaluation of factors η_J and η_δ for the analyzed crack configurations considered next, it is instructive to first examine the ability of the η-factor in describing the relationship between the strain energy for the cracked body and J. The question to be addressed is under what conditions the potential energy change for a cracked body (based upon which J is defined) is equivalent to the plastic work for the stressed cracked body described in terms of the area under the load-displacement curve (based upon which factor η is defined). The energy release rate definition of J given in previous section (see Eq. (1)) represents a mechanical energy balance between the work done by external forces and the strain energy due to the crack. It becomes clear that any plasticity development well outside the crack-tip region provides an additional contribution to the strain energy for the cracked body which therefore affects the plastic area under the load-displacement curve. Under such conditions, the total plastic work does not necessarily translate into a corresponding value of J for the cracked body.

To understand the J vs. plastic work relation for the cracked configurations analyzed here, consider application of the multispecimen procedure outlined before to evaluate the J-integral for the SE(T) fracture specimens under pin load and clamp conditions described previously. Figs. 5 and 6 compare the variation of J with load line displacement (LLD or Δ) for selected specimen configurations which include pin load ($H/W = 6$) and fixed end ($H/W = 10$) conditions with crack sizes in the range: $a/W = 0.1$, 0.2, 0.3 and 0.5. The study focuses on the material with strain hardening exponent $n = 10$ but remains essentially valid for other hardening properties; to conserve space, the results for the $n = 5$ and 20 materials are not shown here. In these plots, the J-values determined directly from the finite element analysis, J_D, based upon a domain procedure provide a baseline value against which the J-values evaluated from the multispecimen strategy outlined previously, J_M, are compared.
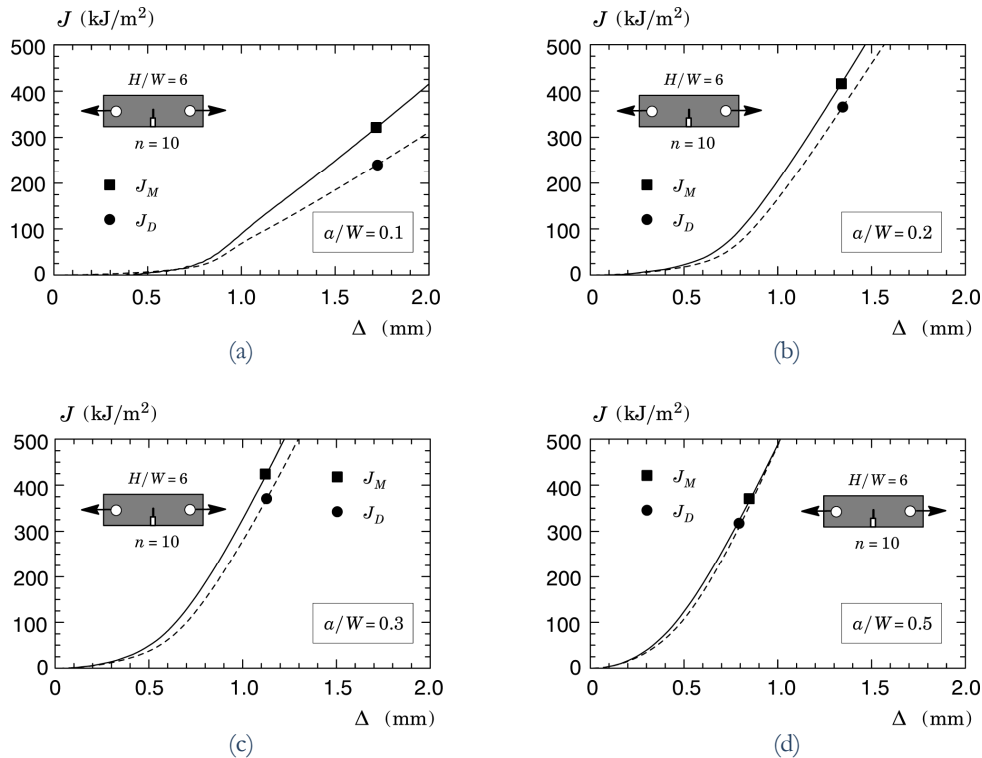
Figure 5: Evolution of J with load-line displacement (Δ) for pin-load SE(T) specimen with $H/W = 6$ and selected a/W-ratios with $n = 10$ material.

The behavior exhibited by the J-trajectories displayed in these plots is consistent with the previous observations about the equivalence between the strain energy for the cracked body and J. For the deeply cracked geometries ($a/W = 0.5$), the J-values computed using the line-integral definition on a remote contour ahead of crack tip are essentially the same as the corresponding values derived from Eq. (17). With decreased crack size, the J-values defined by Eq. (17) increase by an amount ranging from approximately 10% when $a/W = 0.3$ to 30% when $a/W = 0.1$ for the pin-loaded specimen; these differences are similar for the clamped specimen, albeit somewhat smaller. Very similar trends were observed for additional analyses using other material properties ($n = 5$, 20); as already mentioned, these results are not shown here in interest of space.

Given the inherent differences between both procedures and the relative role played by meshing and numerical details in the computed J-values, the observed deviations for the specimen geometries with $a/W = 0.3$ and 0.2 can still be considered acceptable in routine engineering applications. However, the picture is relatively more complex in the case of the very shallow cracked specimen with $a/W = 0.1$. Clearly, the results for this specimen geometry raise concerns as to the effectiveness of the η-method in accurate evaluation of J (and, consequently, CTOD) in current testing protocols for

toughness measurements and defect assessment applications based upon SE(T) fracture specimens with very shallow cracks ($a/W < 0.2$).
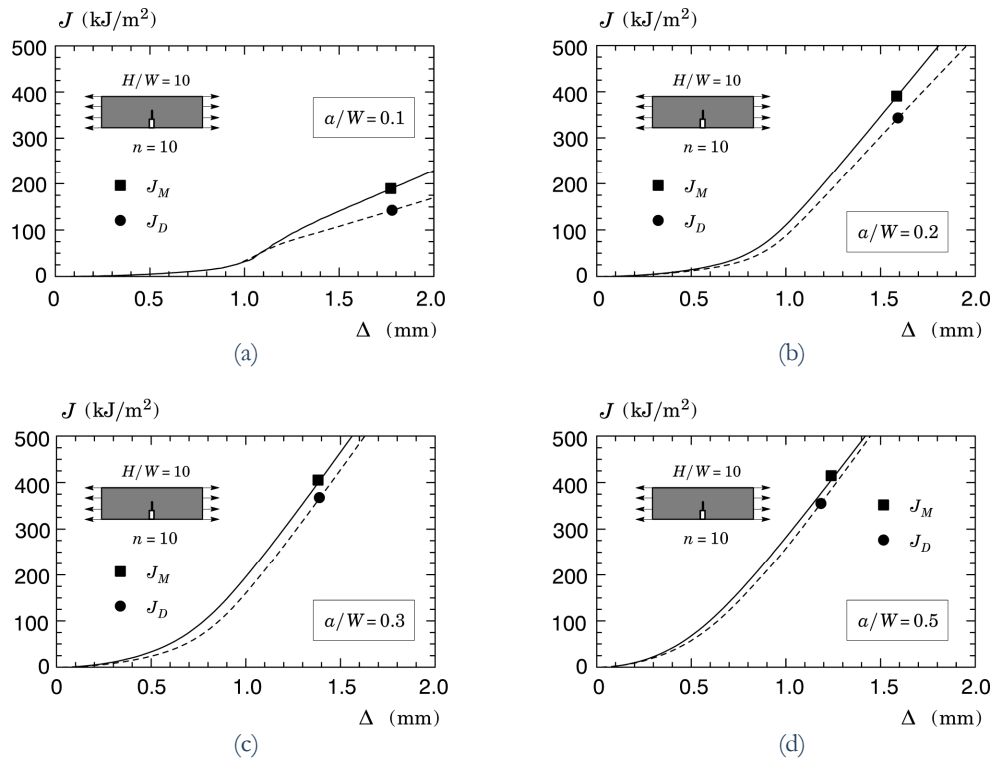
Figure 6: Evolution of J with load-line displacement (Δ) for clamped SE(T) specimen with $H/W = 10$ and selected a/W-ratios with $n = 10$ material.

J AND CTOD ESTIMATION PROCEDURE BASED ON PLASTIC WORK

This section describes the results of the extensive plane-strain analyses performed on models of the pin-loaded and clamped SE(T) described previously. The analyses cover nondimensional η-factors based upon P-CMOD and P-LLD records for the SE(T) fracture specimens with $H/W = 6$ (pin-loaded ends) and $H/W = 10$ (clamped ends).

Figs. 7-9 provide the η-factors corresponding to J and CTOD for the pin-loaded and clamped SE(T) specimens with varying a/W-ratios. In these plots, the solid symbols correspond to the compute η-values whereas the lines represent fitting curves (using a 5-th order polynomial) to the numerical data. Based on the previous findings discussed before in which the effectiveness of the η-method in accurate evaluation of J (and CTOD) for very shallow cracked specimens was questioned, these fitting curves are provided only in the range $0.2 \leq a/W \leq 0.7$.

Consider first the results displayed in Fig. 7(a). The $\eta_{J,P}^{CMOD}$-values for the pin-loaded specimen are relatively independent of strain hardening for the entire range of a/W-ratio, particularly for moderate to low hardening behavior ($n \geq 10$). Such response for this range of hardening exponent suggests approximate estimated values of factor $\eta_{J,P}^{CMOD} \approx 1.0$ for this specimen configuration. The variation of $\eta_{J,C}^{CMOD}$-values with a/W-ratio for the clamped specimen shown in Fig. 7(b) also displays similar trends in which the η-factors are relatively insensitive to strain hardening in the range of moderate to short crack sizes ($a/W \leq 0.3 \sim 0.35$). For deeper cracks, however, there is a slightly more pronounced effect of strain hardening on the η-factors.
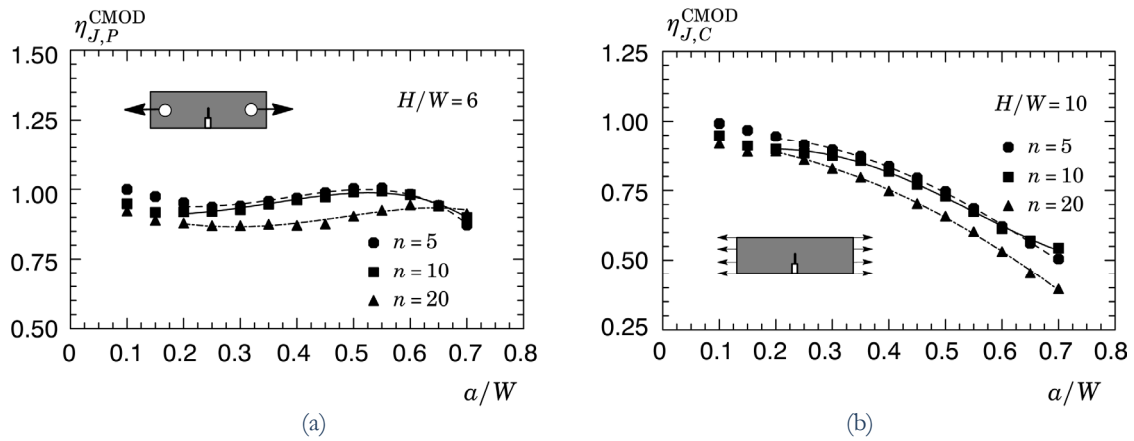
Figure 7: Variation of plastic factor η_J with a/W -ratio derived from CMOD for plane-strain analyses of pin-loaded and clamped SE(T) specimens.
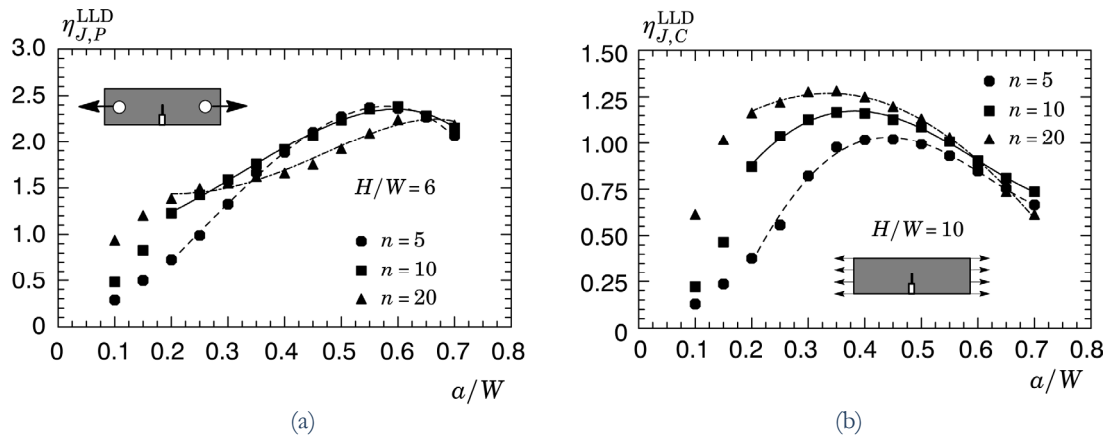
Figure 8: Variation of plastic factor η_J with a/W -ratio derived from LLD for plane-strain analyses of pin-loaded and clamped SE(T) specimens.
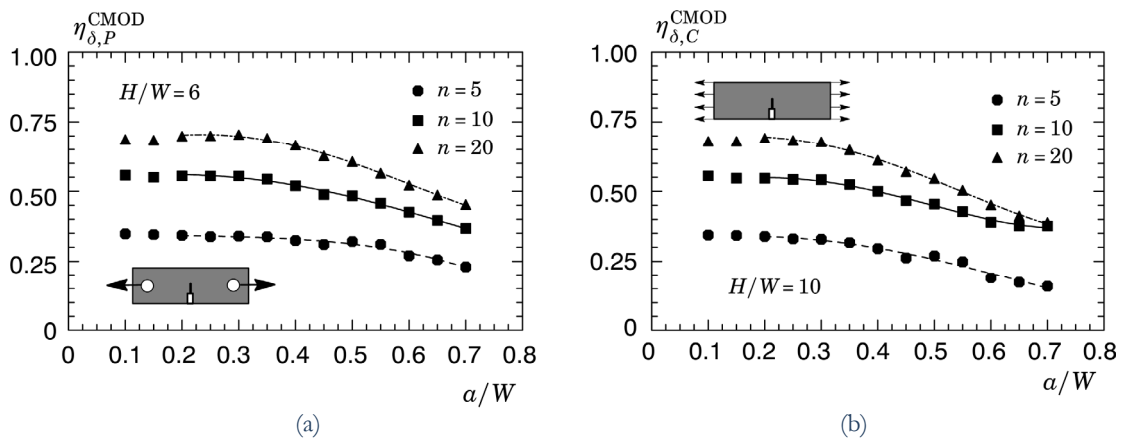
Figure 9: Variation of plastic factor η_δ with a/W -ratio derived from CMOD for plane-strain analyses of pin-loaded and clamped SE(T) specimens.

Fig. 8 presents the η -factors using LLD for the pin-loaded and clamped SE(T) specimens with different a/W -ratios. Here, the η_J^{LLD} -values depend rather strongly on a/W -ratio, particularly in the range $a/W \leq 0.4 \sim 0.5$. Further, factors

η_J^{LLD} are relatively insensitive to strain hardening in the range $a/W \geq 0.4$ for high-to-moderate hardening materials ($n = 5$, 10) but display a larger dependence on strain hardening for shallower cracks, particularly for the clamped specimen with $H/W = 10$.

Consider now the results shown in Fig. 9 . The behavior displayed by the η_δ-values contrasts rather sharply with the previous observed response for factors η_J. Here, both the $\eta_{\delta,P}^{CMOD}$ and $\eta_{\delta,C}^{CMOD}$-values depend rather strongly on the hardening exponent, n. Such feature can simply be explained in terms of the relationship between J and CTOD given by previous Eq. (7) coupled with definition of factor η_δ described by Eq. (10). Because the material's yield stress, which enters directly into Eq. (10), is dependent on the adopted strain hardening exponent, the η_δ-values are also sensitive to the hardening properties. Further, manipulating expressions (7) and (10) and neglecting the elastic components of J and CTOD, one can easily write $\eta_\delta \approx \eta_J/m$ where m is the dimensionless constant relating J and CTOD which is strongly dependent on the material's strain hardening [16,17]. An investigation along this line is progress addressing the relationship between J and CTOD in SE(T) fracture specimens for stationary and growing cracks.

PLASTIC J BASED ON LOAD SEPARATION ANALYSIS

Load Separation Behavior for SE(T) Fracture Specimens

Based on the procedure outlined previously, analysis of the load separation behavior for the plane-strain models of pin-load and clamped SE(T) specimens begins by examining the evolution of load with load-line displacement for the analyzed crack configuration displayed in Fig. 10. Attention is directed to the moderate hardening material with $n = 10$ but the trends are unchanged for other hardening properties. The plots show a rapidly increasing load at low deformation levels and then much more slowly as deformation progresses; essentially similar trends are also observed for the evolution of load with crack mouth opening displacement. Using these results, evaluation of the separation parameter follows from determining the load ratio, S_k, for each specimen geometry based upon the fracture specimen with $a/W = 0.5$ adopted as the reference configuration ($b_0 = 25.4$ mm in the present context). Since the choice of b_0 is rather arbitrary [10,11], the separation behavior is essentially similar for other values of b_0 as the reference specimen size.
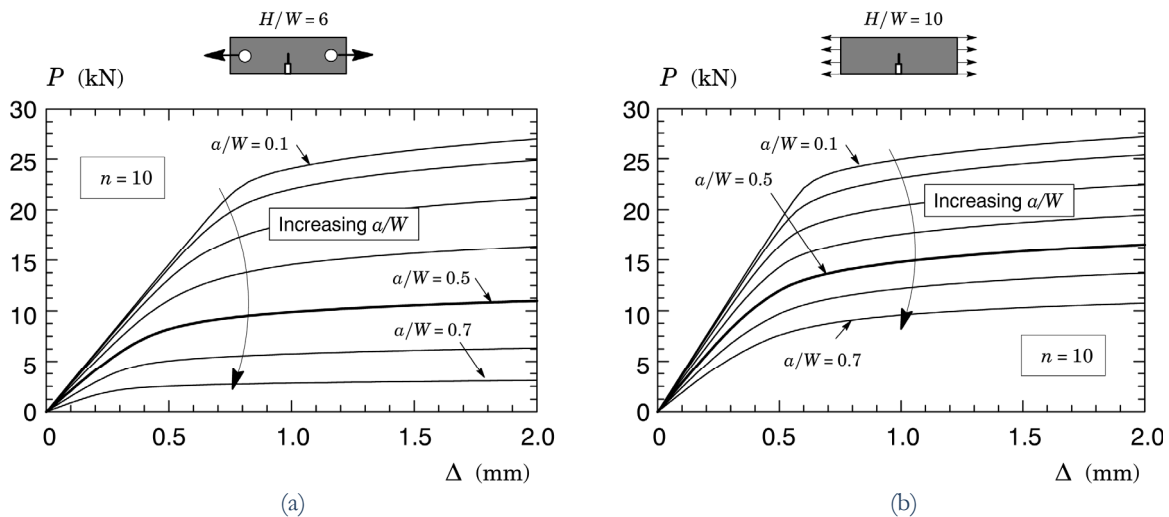
Figure 10: Evolution of load versus load line displacement (LLD) with varying a/W-ratio and $n = 10$ material: a) Pin-loaded specimen with $H/W = 6$; b) Clamped specimen with $H/W = 10$.

Consider now the evolution of S_k^{LLD} with plastic load-line displacement, Δ_p, normalized by the crack ligament size, b_k, for the pin-load and clamped SE(T) specimen displayed in Fig. 11. At very low deformation levels, the elastic component of load-line displacement, Δ_e, has a magnitude which is comparable with the corresponding magnitude of the plastic

component, Δ_p, thereby affecting the computed S_k^{LLD}-value for all specimen geometries and loading conditions (pin-load and clamp); note, however, that since the specimen with $a/W = 0.5$ is taken as the reference configuration, its S_k^{LLD}-value is unaffected. After this short transient, the load ratio S_k^{LLD} is essentially constant for deeply cracked specimens ($a/W \geq 0.4$). For the moderate-to-shallow crack configurations ($a/W \leq 0.3$), parameter S_k^{LLD} displays a little sensitivity on plastic displacement at early stages of loading but which is nevertheless essentially constant with increased Δ_p-values
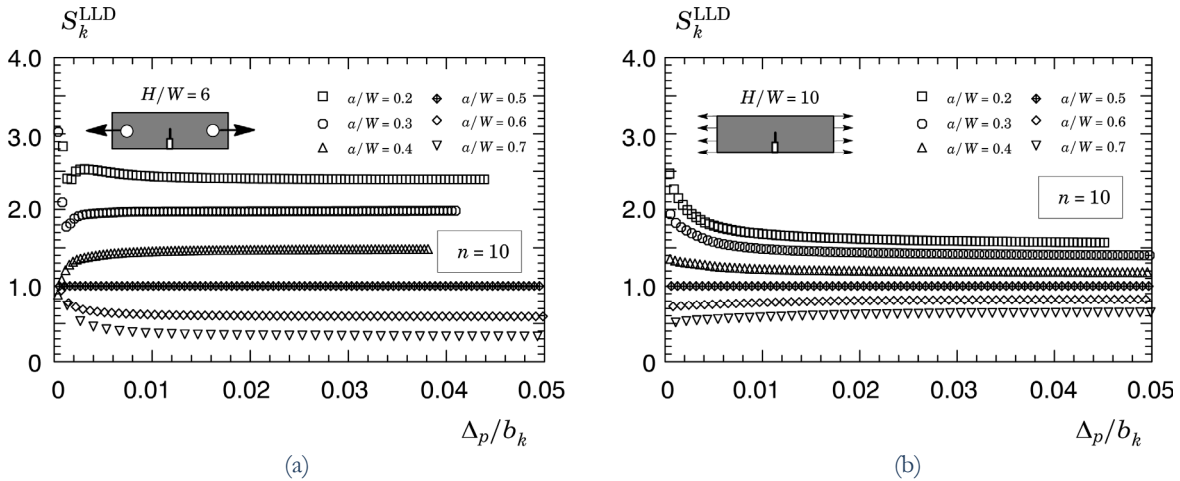
Figure 11: Separation parameter, S_k, with normalized plastic LLD for the $n = 10$ material and varying a/W-ratio: a) Pin-loaded specimen with $H/W = 6$; b) Clamped specimen with $H/W = 10$.

Plastic η-Factors Based on Load Separation Analysis

Before proceeding with the evaluation of factor η based on load separation analysis, a convenient choice for the function $G(b/W)$ (and its derivative) is required so that Eq. (13) can be solved. Using the procedure proposed by Sharobeam and Landes [11], construction of the function $G(b/W)$ follows directly from evaluating $S_k^{LLD}(b/W)$ for each specimen geometry and loading condition so that $G(b/W) = \beta\, S_k^{LLD}(b/W)$, where β is a constant.

Fig. 12 shows the variation of $S_k^{LLD}(b/W)$ with increased values of b/W-ratio (decreased values of a/W-ratio) for the pin-loaded and clamped SE(T) specimens with plastic displacements measured in terms of LLD. To facilitate manipulation of the derivative appearing in Eq. (13), it proves convenient to define a functional relationship for $S_k^{LLD}(b/W)$ by an appropriate fitting of the individual computed S_k-values. In these plots, the solid symbols are the computed S_k-values for each b/W-ratio whereas the lines represent the corresponding fitted curves derived from a standard least square procedure. Here, three fitting functions are adopted to describe the dependence of S_k on b/W: *i*) a power law model (PLF) defined by $S_k = \psi\,(b/W)^\lambda$ in which ψ and λ are constants as proposed by Sharobeam and Landes [11]; *ii*) a 3-rd order polynomial fitting (3PF); *iii*) a 5-th order polynomial fitting (5PF). The trends are clear. The polynomial fitting provides good agreement with each computed individual S_k-value for all analyzed crack configurations and load conditions. In contrast, the power law fitting does not provide a close correspondence with the computed data set for the pin-loaded SE(T) specimen. However, the power law fitting curve matches quite well the variation of S_k with b/W for the clamped SE(T) specimens.

Fig. 13 provides the η_J-factors derived from LLD for the pin-loaded (denoted as $\eta_{J,P}^{LLD}$) and clamped SE(T) specimens (referred to as $\eta_{J,C}^{LLD}$) with varying a/W-ratios. These nondimensional η-values are derived from four different procedures as previously described: *i*) computation of the plastic work defined by the plastic component of the area under

the load vs. LLD curve or the load vs. CMOD curve; *ii)* computation of the load separation parameter, S_k, using a power law fitting (PLF); *iii)* computation of the load separation parameter, S_k, using a 3-rd order polynomial fitting (3PF) and *iv)* computation of the load separation parameter, S_k, using a 5-th order polynomial fitting (5PF) .

(a)   (b)
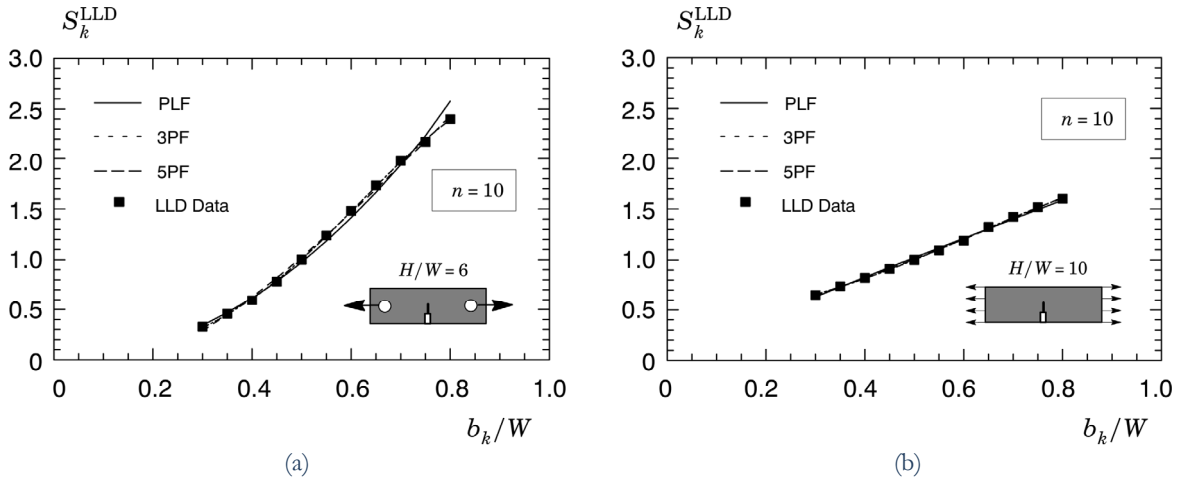
Figure 12: Variation of separation parameter, S_k, derived from LLD with b/W-ratio for the $n = 10$ material and different fitting functions: a) Pin-loaded specimen with $H/W = 6$; b) Clamped specimen with $H/W = 10$.

(a)   (b)
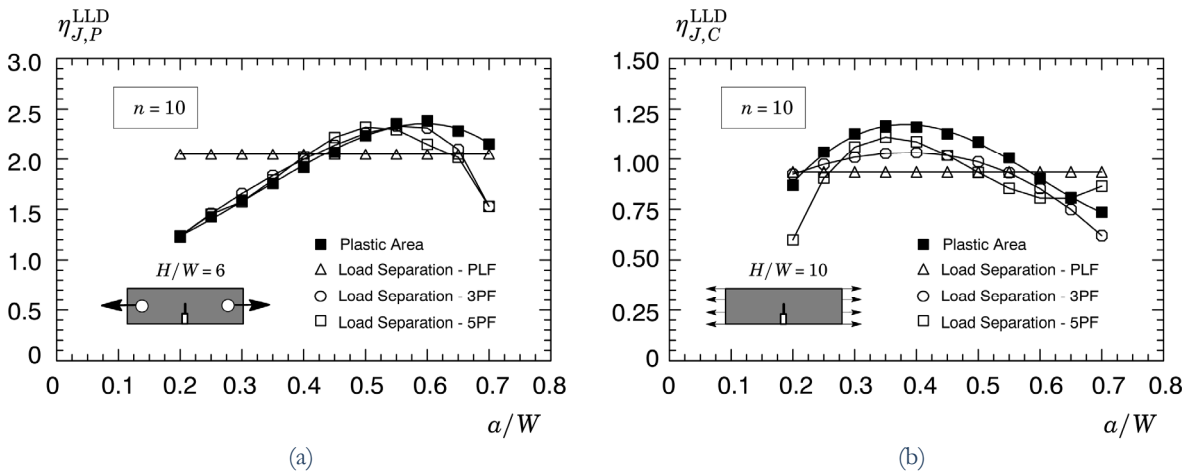
Figure 13: Comparison of plastic factors η_J derived from LLD for pin-loaded and clamped SE(T) specimens based on different estimation procedures.

Considering the results displayed in Fig. 13 based on LLD data, the significant features include: *i)* a good agreement is observed between the η-values derived from the plastic area approach and the load separation procedure using a polynomial fitting for the analyses based upon LLD records for the pin-loaded specimens, particularly in the range $0.2 \leq a/W \leq 0.6$; *ii)* differences in the η-factors derived from the plastic area method and the load separation procedure using a polynomial fitting are slightly larger for the clamped specimens; *iii)* the η-factors derived from the load separation analysis using a power law fit is independent of crack size.

One salient feature of the previous results is the independence of factor η_J^{LLD} on crack size for any condition analyzed. As already hinted before, this is not unexpected and can be easily understood by the following argument. A simples inspection of previous Eq. (13) reveals that function $G(b/W)$ (which is proportional to $S_k(b/W)$) cancels when a power law type model is employed. Consequently, the assumption of a power law in the form $S_k = \psi(b/W)^\lambda$ adopted by Sharobeam and Landes [11] with parameters ψ and λ translates directly into a constant η-factor which is equal to the

power law coefficient, λ. Such conclusion is in stark contrast with previous work conducted by other researchers (see, e.g., [24] and references therein) and the results presented here which reveal a rather strong dependence of factor η on crack size, particularly for moderate-to-shallow cracks ($a/W \leq 0.3$).

CONCLUSIONS

The extensive numerical analyses conducted for pin-loaded and clamped SE(T) fracture specimens provide a large set of plastic η-factors applicable to evaluate J and CTOD with varying a/W-ratios and hardening properties characteristic of structural, pressure vessel and pipeline steels. These dimensionless η-values enter directly into estimation procedures for fracture toughness based on experimentally measured plastic work as represented by the plastic area under the load-displacement curve derived from current testing protocols. The analyses also considered alternative approaches to evaluate the plastic component of the J-integral from laboratory testing of conventional fracture specimens using the load separation methodology and the multispecimen procedure.

The present analyses also demonstrate good agreement between the J-integral determined from plastic work and its domain integral definition for shallow to deep crack SE(T) specimens ($a/W \geq 0.2$). While the studies conducted here do not recommend testing very shallow cracked tensile specimens ($a/W < 0.2$) due to additional complexities and low accuracy in J measurements, the plane-strain results reported in this work clearly lend strong support for estimation procedures of J and CTOD toughness parameters based on plastic work and the associated η-factor. Overall, the present investigation, when taken together with previous studies, provide a fairly extensive body of results which serve to determine parameters J and CTOD for different materials using tensile SE(T) specimens with varying geometries and loading conditions. On-going work on other related fronts is in progress which includes the assessment of weld strength mismatch effects on J-based procedures for J and CTOD evaluation, and development of robust relationships between J and CTOD in SE(T) fracture specimens for stationary and growing cracks.

ACKNOWLEDGMENTS

REFERENCES

[1] American Society for Testing and Materials, Standard Test Method for Measurement of Fracture Toughness, ASTM E1820, (2008).
[2] J. W. Hutchinson, Journal of Applied Mechanics, 50 (1983) 1042.
[3] G. H. B. Donato, C. Ruggieri, In: ASME International Conference on Offshore Mechanics and Arctic Engineering (OMAE 2008), American Society of Mechanical Engineers, (2008).
[4] S. Cravero, C. Ruggieri, Engineering Fracture Mechanics, 72 (2005) 1344.
[5] L. A. L. Silva, S. Cravero, C. Ruggieri, Engineering Fracture Mechanics, 73 (2006) 2123.
[6] J. D. G. Sumpter, C. E. Turner, In: Cracks and Fracture, American Society for Testing and Materials, ASTM STP 601 (1976) 3.
[7] V. Kumar, M. D. German, C. F.Shih, An Engineering Approach to Elastic-Plastic Fracture Analysis, EPRI Report NP-1931, Electric Power Research Institute, Palo Alto, CA, (1981).
[8] N. E. Dowling, Mechanical Behavior of Materials, 2nd Edition, Prentice Hall, NJ (1999).
[9] A. Zahoor, EPRI Report NP-6301-D, Electric Power Research Institute, 2 (1989).
[10] P. C. Paris, H. Ernst, C. Turner, In: Fracture Mechanics: Twelfth Conference, American Society for Testing and Materials , ASTM STP, 700 (1980), 338.

[11] M. Sharobeam, J. D. Landes, International Journal of Fracture, 41 (1991) 81.

[12] M. F. Kanninen, C. H. Popelar, Advanced Fracture Mechanis, Oxford University Press, New York (1985).

[13] J. W. Hutchinson, P. C. Paris, In: Elastic-Plastic Fracture, American Society for Testing and Materials, ASTM STP, 668 (1979) 37.

[14] S. Cravero, C. Ruggieri, International Journal of Fracture, 148 (2008) 387.

[15] J. R. Rice, P. C. Paris, J. G. Merkle, In: Progress in Flaws Growth and Fracture Toughness Testing, American Society for Testing and Materials, ASTM STP 536, (1973) 231.

[16] M. T. Kirk, R. H. Dodds, Journal of Testing and Evaluation, 21 (1993) 228.

[17] C. F. Shih, Journal of the Mechanics and Physics of Solids, 29 (1981) 305.

[18] T. L. Anderson, Fracture Mechanics: Fundaments and Applications - 3rd Edition, CRC Press, Boca Raton, 2005.

[19] British Standard, Fracture Mechanics Toughness Tests, BS 7448 (1991).

[20] J. A. Begley, J. D. Landes, In: Fracture Toughness, American Society for Testing and Materials, ASTM STP 514, (1972) 1.

[21] A. Gullerud, K. Koppenhoefer, A. Roy, S. RoyChowdhury, M. Walters, B. Bichon, K. Cochran, R. H. Dodds, Structural Research Series (SRS) 607, UILU-ENG-95-2012, University of Illinois at Urbana-Champaign (2004).

[22] B. Moran, C. F. Shih, International Journal of Fracture, 35 (1987) 295.

[23] C. Ruggieri, FRACTUS2D: Numerical Computation of Fracture Mechanics Parameters for 2-D Cracked Solids, EPUSP, University of São Paulo (2010).

[24] S. Cravero, C. Ruggieri, Engineering Fracture Mechanics, 74 (2007) 2735.